

# Redatuming physical systems using symmetric autoencoders

Pawan Bharadwaj\*

Indian Institute of Science, CV Raman Rd, Bengaluru, Karnataka 560012, India.

Matthew Li and Laurent Demanet

Massachusetts Institute of Technology, 77 Massachusetts Avenue, Cambridge, MA 02139, USA.

(Dated: March 28, 2022)

This paper considers physical systems described by hidden states and indirectly observed through repeated measurements corrupted by unmodeled nuisance parameters. A network-based representation learns to disentangle the coherent information (relative to the state) from the incoherent nuisance information (relative to the sensing). Instead of physical models, the representation uses symmetry and stochastic regularization to inform an autoencoder architecture called SymAE. It enables redatuming, i.e., creating virtual data instances where the nuisances are uniformized across measurements.

## INTRODUCTION

In contemporary sciences, there is increasing reliance on experimental designs involving measurements that are corrupted by unmodelled and uncontrollable *nuisance variations*. For example, in geophysics, specifically passive time-lapse seismic monitoring, the recorded seismic waves are generated by uncontrollable sources related to: tectonic stress changes in the subsurface [1] or ocean-wave activity [2]. Similarly, in astronomy, the spectral lines in the fluorescent emissions that characterize the chemical composition of the lunar surface fluctuate depending on unmodelled solar flares [3, 4]. Such designs introduce ambiguity to the experimentalist when determining whether changes in data represent *coherent information*, i.e., the signal related to the underlying physical state, or conversely represent *nuisance information*, i.e., the noise related to data acquisition. Nevertheless, these uncontrollable experiments (along with others listed in Tab. I) remain the only feasible avenue to measure and study certain physical phenomena; thereby, motivating the development of tools to reliably disentangle the nuisances in these settings.

Fortunately, a redeeming feature of this class of experiments is the abundant production of the measurements describing the same physical state, albeit with different nuisance variations. We refer to these repeated measurements as *instances*. Access to a sufficiently dissimilar collection of instances, in principle, enables disentanglement of coherent information from nuisance information without a reference to the underlying physical model [5]. Therefore, our approach aims to decompose each measurement into separate *latent codes* which are correlated, but typically not equivalent, to the corresponding (unknown) parametric representations underlying both sources of information. The coherent and nuisance latent codes are determined from an auto-encoding architecture with an encoder (which maps into the latent space) and a decoder that reconstructs the data in a near-lossless fashion. Our approach avoids explicit modeling of the physics and the nuisances. This framework can be seen as a vast generalization of multichannel blind deconvolution [6], where neural networks replace the convolutional signal model; the coherent information replaces the unknown source, and the nuisance variations correspond to the unknown filters.

Disentanglement into coherent and incoherent latent variables enables a reliable comparison of coherent information between instances describing different states. It also relegates analysis into a latent space that is abstractly related to the physical system. We propose an additional mechanism, namely redatuming, to convert from latent coordinates back to the nominal data space. It involves the combination of coherent information from one instance with the nuisance information from a reference instance — this synthesizes a *virtual* instance that is not originally measured. The relevance of such virtual data instances is that they can be engineered to share their nuisance information with another (measured) data instance so that any remaining discrepancy can be solely explained from differences in the underlying coherent physical states. Alternatively, this entire process can be viewed as “swapping the physics” between states. We conjecture that this new type of redatuming can help rethink how to approach inverse problems with significant uncertainties in the forward model.

To illustrate redatuming, we revisit the example of time-lapse geophysical subsurface monitoring that is detailed in Tab. I and appendix. Here, the goal is to detect changes in complex heterogeneous subsurface [16], plotted as “state #1” and “state #2” along the abscissa of Fig 1. In seismic experiments, the mechanical properties (dependent

---

\* Formerly at Massachusetts Institute of Technology, USA.

TABLE I. A representative list of experiments, where numerous instances are measured at each state that describes the physical phenomenon of interest. The instances exhibit dissimilarities due to the nuisance variations while sharing coherent information about the state.

experiment; goal is to characterize the variation of ...	measured instances in each state comprise ...	components of information in each instance	
		coherent information describing the state	nuisance information
seismic time-lapse imaging; subsurface with time [7, 8]	waves propagating through a given subsurface region, but generated by different uncontrollable sources	mechanical properties of the subsurface region	source signature, location and mechanism
seismology; source mechanism among different earthquakes [9, 10]	waves from an earthquake measured at different receivers	earthquake’s spectrum, geology near epicenter region, etc.	multipathing in the subsurface, Doppler effects from rupture propagation, etc.
lunar X-ray fluorescence spectroscopy; lunar geology with location [4, 11]	fluorescence from regions that share a given rock type under different solar conditions	elemental composition of the rock type	solar-flare information
asteroseismology [12, 13]; pulsating mechanism among Rapidly oscillating Ap [14] or Delta Scuti [15] stars	brightness of a given star measured in different temporal windows	physics that is symmetrical under time translation, e.g., star’s internal structure, kappa opacity mechanism, etc.	short-lived excitation mechanisms, e.g., surface convection, variable radial velocity, etc.

on distance  $x$  and depth  $z$ ) of the medium are indirectly observed when sources illuminate them with elastic waves. The measured instances constitute the time-dependent (indexed using  $t$ ) wavefield recorded at a given set of receivers (indexed using  $r$ ) in the medium — plotted in Figs. 1a and 1c. Note that the structural complexities of the media will lead to multipath wave propagation. As the sources are uncontrollable with randomized signatures and locations, i.e., the nuisance variations along the ordinate of Fig 1, the detection goal is confounded. For example, a direct comparison of the measured instances to extract localized changes (marked using a blue arrow) corresponding to the medium is difficult. Therefore, redatuming is used to replace the subsurface information of Fig 1a with that of Fig 1c while retaining its source information. This generates the *virtual* instance, plotted in Fig. 1d, which can be subtracted from the suitable measured instance to access the subsurface changes (via standard imaging). In other words, after redatuming, the domain expert can perform data analysis using traditional tools without reference to the implicit latent space. Finally, note that the virtual instances have a low relative mean-squared error in comparison to instances that are simulated using appropriate source and medium parameters.

These ideas are inspired by recent machine learning literature where redatuming is instead referred to as *styling*, see e.g., [17–19], and the reliance on multiple instances is referred to as *weak supervision* [5, 20]. However, we note that these communities primarily apply these tools to images with significant visual structure, e.g. wherein nuisance information relates to the “image style”, and the coherent information relates to the “image content” — we presented redatuming of MNIST digits in the appendix. This letter instead introduces the idea of redatuming to scientific signals. Most critically, in this setting we are able to quantify the accuracy of virtual instances by comparison to explicit synthetic models.

## OUR CONTRIBUTIONS

To achieve redatuming, we propose an unsupervised deep-learning architecture called symmetric autoencoder (SymAE). Achieving the requisite disentangled latent representation with SymAE requires two deliberate architectural design choices: 1. The encoder for the coherent latent variables is constrained to be symmetric with respect to the ordering of the instances indexed by nuisance variations. 2. The remaining latent-code dimensions are orthogonalized by stochastic regularization that promotes dissimilarity among the instances [21]. Therefore, these remaining latent components are designed to *not* represent the coherent information and correspond only to the nuisance variations.

With this latent structure, redatuming is equivalent to swapping the coherent codes in the latent space before decoding to produce a virtual instance. In the appendix, we provide numerical evidence that SymAE’s redatuming preserves and captures the salient features of the underlying physical modeling operator, thus enabling the use of virtual datapoints for subsequent downstream tasks such as parameter estimation. For example, a low relative mean-squared error in the virtual instances of Fig 1 confirms that SymAE’s redatuming is consistent with the physics of wave propagation.

Redatuning already appears in the context of traditional seismic inversion [22–26]. The major differences with our generalized approach, however, are: 1. the seismic-specific redatuning is limited to swapping sources or receivers from one state to another — SymAE can swap any information as long as it is coherent across the instances; 2. seismic redatuning uses physics-based formulas with convolutions or cross-correlations — in contrast, SymAE derives the redatuning operators from the recorded data in an unsupervised manner, unlocking processing for far more general situations than cross-correlations allow. We refer the reader to [27–29] for examples of analytical-based redatuning applied to specific geophysical settings.

## DATAPOINTS AND NOTATION

In this section, we describe the training set  $\{X_i\}_{i=1,\dots,n_X}$  that SymAE encodes to produce a compressed and disentangled representation. As mentioned above, each datapoint  $X_i$  must contain multiple instances that repeatedly capture the same physical state  $\epsilon_i$ . We uniformly sample from 1 to  $n_\epsilon$  to generate the state labels  $\{\epsilon_i\}_{i=1,\dots,n_X}$  for our synthetic experiments — in practice, the experimental conditions determine this sampling distribution. We emphasize that knowledge of the state labels is *not* necessary for either training or testing since our framework is purely unsupervised. Each  $X_i$  contains  $n_\tau$  instances which we index as  $X_i[\tau]$  for  $\tau = 1, \dots, n_\tau$  such that  $X_i = [X_i[1]; \dots; X_i[n_\tau]]$ . The individual instances  $X_i[\tau]$  are abstractly  $k$ -dimensional vectors, i.e.  $X_i[\tau] \in \mathbb{R}^k$ . The determination of  $k$  is specific to each experiment; for example, in the instance depicted in Fig 1a the dimension  $k$  is the product of the number of receivers  $r$  and length of the time series  $t$ . In our notation,  $[A; B]$  denotes a vertical concatenation of two vectors  $A$  and  $B$ . Again, the collection of instances  $\{X_i[\tau]\}_{\tau=1,\dots,n_\tau}$  for a fixed index  $i$  shares the same coherent information to the state  $\epsilon_i$  but vary by  $\tau$ -specific nuisance variations. For brevity we omit the subscript for the datapoint  $X_i$  and state  $\epsilon_i$  whenever the context is clear.

## ARCHITECTURE

We refer the reader to [30] for an accessible tutorial on autoencoders [31]. Functionally, autoencoders are comprised of two components: an encoder **Enc** that maps datapoint  $X_i$  into latent code  $H_i = \text{Enc}(X_i)$ , and a decoder **Dec** that attempts reconstruct to  $X_i$  from the code. Traditionally, both functions **Enc** and **Dec** are determined by minimizing the reconstruction loss

$$\text{Enc, Dec} = \arg \min_{\text{Enc, Dec}} \sum_i \|X_i - \text{Dec}(\text{Enc}(X_i))\|^2 \quad (1)$$

over the training dataset. When non-linear parameterizations are used for both **Enc** and **Dec**, the latent representation no longer describes the geometry of the datasets using linear subspaces [32]. However, this representation can efficiently compress the information [33].

SymAE builds on non-linear autoencoders but requires additional technical ingredients. A direct application of the traditional autoencoding ideas will not ensure that the coherent and nuisance information are encoded into separate components (dimensions) in the latent space. To achieve this separation, SymAE relies on the unique encoder structure as depicted in Fig. 2. Additionally, we provided Tensorflow-style [34] algorithms in the appendix that detail the implementation of SymAE. The encoder structure can be mathematically described by

$$\text{Enc}(X) = [\text{CEnc}(X); \text{NEnc}(X[1]); \dots; \text{NEnc}(X[n_\tau])]. \quad (2)$$

At a high level, this produces a latent code  $H$  which is partitioned into interpretable components. Specifically, each datapoint  $X = [X[1]; \dots; X[n_\tau]]$  is represented into a structured latent code  $H = [C; N[1]; \dots; N[n_\tau]]$  where the sub-components  $C = \text{CEnc}(X)$  contain coherent information in  $X$  while the remaining sub-components  $N[\tau] = \text{NEnc}(X[\tau])$  complement this with instance-specific nuisance information. Note the dimensions of the latent codes  $C \in \mathbb{R}^p$  and  $N[\cdot] \in \mathbb{R}^q$  do not need to coincide and are user-specified hyperparameters.

Subsequently, SymAE’s decoder **Fuse** non-linearly combines code  $C$  with each instance-specific code  $N[\cdot]$  to reconstruct the original datapoint, instance-by-instance, viz.

$$\begin{aligned} \hat{X} &= \text{Dec}(H) = \text{Dec}([C; N[1]; \dots; N[n_\tau]]) \\ &= [\text{Fuse}([C; N[1]]); \dots; \text{Fuse}([C; N[n_\tau]])]. \end{aligned} \quad (3)$$

We do not enforce any constraints on **Fuse** in our experiments and parametrize it with standard deep learning building blocks [35].

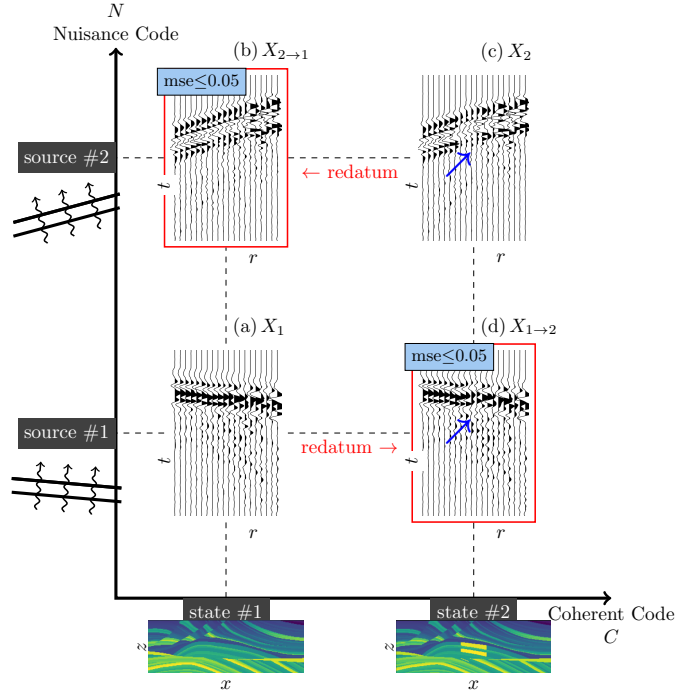


FIG. 1. Redatuning is equivalent to swapping the coherent and nuisance information in SymAE’s latent space. Here, as SymAE learns to represent the information on medium (coherent) and incoming plane-wave sources (nuisance) separately, the recorded wavefield (a and c) in a seismic experiment (see Tab. I) can be redatumed to generate virtual measurements (b and d). A low error is confirming that the redatuming operator captures salient features of the wave-equation modeling despite a multipath propagation due to the complex medium inhomogeneities.

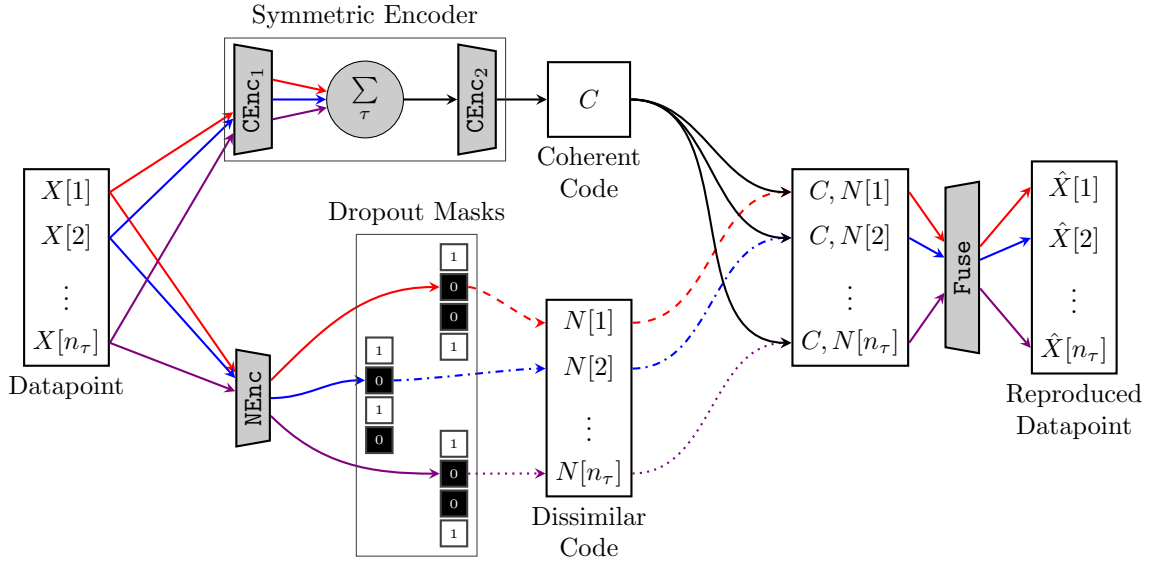


FIG. 2. Architecture of symmetric autoencoder. The information that is coherent across the instances of a datapoint can only propagate through the network via solid arrows — notice the stochastic regularization employed to prevent its propagation. We used colored arrows to indicate the propagation of the remaining instance-specific nuisance information — notice that a symmetric function, i.e., symmetric w.r.t. the order of the instances, prevents its propagation. As a result, the autoencoder disentangles the coherent information from the nuisance variations in the latent space.

To ensure **CEnc**, the *coherent encoder*, only encodes the coherency or similarity among the instances in  $X$  we constrain it to be invariant under permutations of the instances of a same state. In other words, for all permutations  $\Pi$  along the instance dimension, we desire that

$$C = \mathbf{CEnc}(X) = \mathbf{CEnc}(X[\Pi(1:n_\tau)]) \quad (4)$$

purely represents the coherent information since  $C$  does not depend on the labeling of the instances in  $X$ . On the other hand, the nuisances are dissimilar across instances and thus cannot be encoded using **CEnc** without significant loss of information.

SymAE’s coherent encoder explicitly achieves the invariance mentioned above using permutation-invariant network architectures following [36] which provide universal approximation guarantees for symmetric functions. The data due to each source instance are first transformed using **CEnc**<sub>1</sub> and summed along the instance dimension. This output is then processed by **CEnc**<sub>2</sub> resulting in

$$C = \mathbf{CEnc}_2 \left( \frac{1}{n_\tau} \sum_{\tau=1}^{n_\tau} \mathbf{CEnc}_1(X[\tau]) \right). \quad (5)$$

This comprises the network architecture of **CEnc**. In our experiments the functions **CEnc**<sub>1</sub> and **CEnc**<sub>2</sub> are parametrized by compositions of fully connected layers and convolutional layers. We emphasize that the key observation in eq. 5 is that the summation of the *transformed instances*  $\mathbf{CEnc}_1(X_i[\tau])$  is symmetric with respect to the ordering of instances. This ensures that the desired symmetry (eq. 4) is achieved. Alternative symmetric functions such as the max function can be used in place of summation; we refer to [37] for a review of various permutation-invariant architectures.

In contrast, the purpose of **NEnc** is to encode the nuisance information specific to each instance of the datapoint while ignoring coherent information. The latter aspect is a significant concern as we do not want the decoder **Fuse** to ignore the  $C$  component in favour using purely  $N[\cdot]$  information for reconstruction. To this end, during training of SymAE we introduce *stochastic regularization* to the output of the nuisance encoder viz,

$$N[\tau] = \mathbf{NEnc}(X[\tau]) + \text{“strong noise”}. \quad (6)$$

In our experiments, we implement this noise using either Bernoulli dropout regularization [38] with probability  $p$  or Gaussian dropout with unit mean and  $p(1-p)$  variance [39, 40]. In either case, the strength of the noise is proportional to  $p$ , which is a hyperparameter which the user must tune. Intuitively, by randomly obfuscating elements of  $N$  via noise, the decoder views the codes as dissimilar to each other, thereby failing to reconstruct any coherent information from  $N$ . Critically, however, each  $N$  must still be expressive enough to encode nuisance-specific information. The balance between regularization strength  $p$  and the dimension (i.e., expressivity) of the latent codes is user-determined on an external validation set. The SymAE components **NEnc**, **CEnc** and **Fuse** are trained concurrently by minimizing Eq. 1 with the regularization mechanism just described. Note that stochastic regularization is not employed at test-time so that the entirety of the  $N$  codes are seen unaltered by the decoder.

Finally, note that we only constrained the encoders to avoid “cross-talk” while disentangling the coherent and nuisance information. Implicitly the success of SymAE, therefore, requires a sufficiently large number of instances with *dissimilar* nuisance variations in order to achieve the desired structure of the latent space. We leave an examination of characterizations of physical models which are amenable to disentanglement to future work.

## REDATUMING INTO VIRTUAL INSTANCES.

A trained SymAE learns a representation with disentangled coherent and nuisance information. Redatuming data becomes equivalent to manipulations in the latent space — as illustrated in the Fig. 1, where virtual instances are generated by swapping latent coordinates. In general, the coherent information in the  $\tau$ -th instance of a datapoint  $X_i$  can be swapped with that of another datapoint  $X_j$  using

$$\hat{X}_{i \rightarrow j}[\tau] = \mathbf{Fuse}([\mathbf{CEnc}(X_j); \mathbf{NEnc}(X_i[\tau])]). \quad (7)$$

Here,  $X_j$  is an observation of a different state compared to  $X_i$ . Notice that the nuisance information in the virtual datapoint  $\hat{X}_{i \rightarrow j}$  is identical to that of original datapoint  $X_i$ . Consequently, we attribute the difference between  $X_i$  and  $\hat{X}_{i \rightarrow j}$  to the changes between the physical states. As a demonstration, the observed and virtual instances from the seismic experiment are embedded into the SymAE’s latent space in Fig. 1.

## CONCLUSIONS.

We propose an autoencoder architecture for poorly controlled scientific experiments that produce an abundance of incompletely modeled measurements of a physical system. The autoencoder learns a data representation that disentangles the coherent information inherent to the physical state, from the nuisance modifications inherent to the experimental configuration, in a model-free fashion. Two ideas are critical: 1. leveraging symmetry under reordering of the data instance in order to represent the coherent information in a first encoder, and 2. stochastic regularization in order to prevent coherent information from being represented by the second encoder. As a result, the architecture can perform redatuming, i.e., the swapping of physics in order to create virtual measurements.

### Appendix A: Algorithms

These Tensorflow-style [34] algorithms provide further details on the implementation of SymAE. **ConvA** and **Conv** denote convolutional layers with and without activation, respectively. We used **distribute** to apply the same layer to each of the instances. For a given application, hyperparameters to be tuned are: filters and kernel sizes of the convolutional layers, length of nuisance code  $n_N$ , length of the coherent code  $n_C$ , and the dropout rate  $\alpha$ .

---

#### Algorithm 1: Keras-style algorithm for preparing coherent encoder CEnc.

---

1: $C \leftarrow \text{distribute}(\text{ConvA})(X)$ ; $C \leftarrow \text{distribute}(\text{ConvA})(C)$ ; $C \leftarrow \text{distribute}(\text{MaxPool})(C)$	{CEnc <sub>1</sub> }
2: $C \leftarrow \text{distribute}(\text{ConvA})(C)$ ; $C \leftarrow \text{distribute}(\text{ConvA})(C)$ ; $C \leftarrow \text{distribute}(\text{MaxPool})(C)$	{CEnc <sub>1</sub> }
3: $C \leftarrow \text{reduce\_mean}(C, \text{axis} = 1)$	{sum over instances}
4: $C \leftarrow \text{ConvA}(C)$ ; $C \leftarrow \text{ConvA}(C)$ ; $C \leftarrow \text{MaxPool}(C)$	{CEnc <sub>2</sub> }
5: $C \leftarrow \text{ConvA}(C)$ ; $C \leftarrow \text{ConvA}(C)$ ; $C \leftarrow \text{BatchNormalization}(C)$	{CEnc <sub>2</sub> }
6: $C \leftarrow \text{MaxPool}(C)$ ; $C \leftarrow \text{Flatten}(C)$ ; $C \leftarrow \text{Dense}(C, n_C)$	{CEnc <sub>2</sub> }
7: $\text{CEnc} = \text{Model}(X, C)$	

---



---

#### Algorithm 2: Keras-style algorithm for preparing nuisance encoder NEnc.

---

1: $N \leftarrow \text{distribute}(\text{ConvA})(X)$ ; $N \leftarrow \text{distribute}(\text{ConvA})(N)$ ; $N \leftarrow \text{distribute}(\text{MaxPool})(N)$	
2: $N \leftarrow \text{distribute}(\text{ConvA})(N)$ ; $N \leftarrow \text{distribute}(\text{ConvA})(N)$ ; $N \leftarrow \text{distribute}(\text{MaxPool})(N)$	
3: $N \leftarrow \text{distribute}(\text{ConvA})(N)$ ; $N \leftarrow \text{distribute}(\text{ConvA})(N)$ ; $N \leftarrow \text{distribute}(\text{MaxPool})(N)$	
4: $N \leftarrow \text{distribute}(\text{ConvA})(N)$ ; $N \leftarrow \text{distribute}(\text{ConvA})(N)$	
5: $N \leftarrow \text{distribute}(\text{BatchNormalization})(N)$	
6: $N \leftarrow \text{distribute}(\text{MaxPool})(N)$ ; $N \leftarrow \text{distribute}(\text{Flatten})(N)$ ; $N \leftarrow \text{distribute}(\text{Dense})(N, n_N)$	
7: $\text{NEnc} = \text{Model}(X, N)$	

---



---

#### Algorithm 3: Fuse latent codes $C$ and $N$ .

---

1: $\hat{N} \leftarrow \text{dropout}(N, \alpha)$	{stochastic regularization}
2: $\hat{C} = \text{RepeatVector}(n_r)(C)$ ; $\hat{X} \leftarrow \text{concatenate}([\hat{C}, \hat{N}], \text{axis} = 2)$	{distribute coherent code to each instance}
3: $\hat{X} \leftarrow \text{distribute}(\text{Dense}(n_r \times n_t))(\hat{X})$ ; $\hat{X} \leftarrow \text{distribute}(\text{Reshape}(n_r, n_t, 1))(\hat{X})$	
4: $\hat{X} \leftarrow \text{distribute}(\text{ConvA})(\hat{X})$ ; $\hat{X} \leftarrow \text{distribute}(\text{ConvA})(\hat{X})$ ; $\hat{X} \leftarrow \text{distribute}(\text{ConvA})(\hat{X})$	
5: $\hat{X} \leftarrow \text{distribute}(\text{BatchNormalization})(\hat{X})$ ; $\hat{X} \leftarrow \text{distribute}(\text{ConvA})(\hat{X})$	
6: $\hat{X} \leftarrow \text{distribute}(\text{Conv})(\hat{X})$	{output datapoint}

---

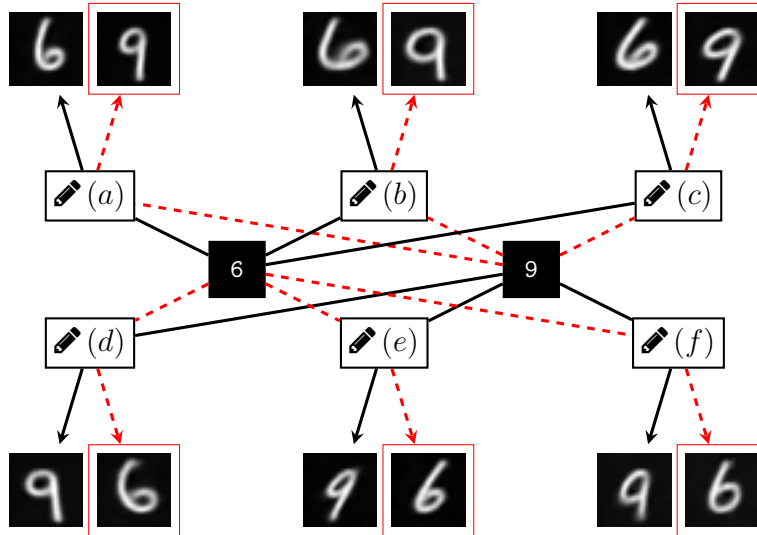


FIG. 3. In the MNIST experiment, SymAE helps generation of virtual instances by swapping the digit (coherent) information from the images (6 and 9 plotted here). (a)–(c) Instances of digit 6 exhibit dissimilarities due to the writing style (nuisance), where the digit information is swapped with 9 as depicted using the dashed lines. Similarly, notice that the virtual instances in (d)–(f) contain the same style as in the original images, except with another digit.

## Appendix B: MNIST Experiment

This section illustrates SymAE’s redatuming using the MNIST hand-written digit dataset. Here, the instances correspond to the hand-written images from a given class (analogous to the physical state). In each class, the digit information is coherent with nuisance variation in hand-writing style. The goal is to track the digit information across these classes without hindrance due to the writing style. The dataset consists of 60,000 training images and 10,000 test images with digit labels. For this dataset, every image has a total of  $28 \times 28 = 784$  pixels, and the intrinsic dimensionality is known to be 10. After sorting the images into ten-digit states, we generated a total of 10000 datapoints. Fig. 3 demonstrates that SymAE facilitates the generation of virtual images after swapping the digit information while retaining the style of a particular image.

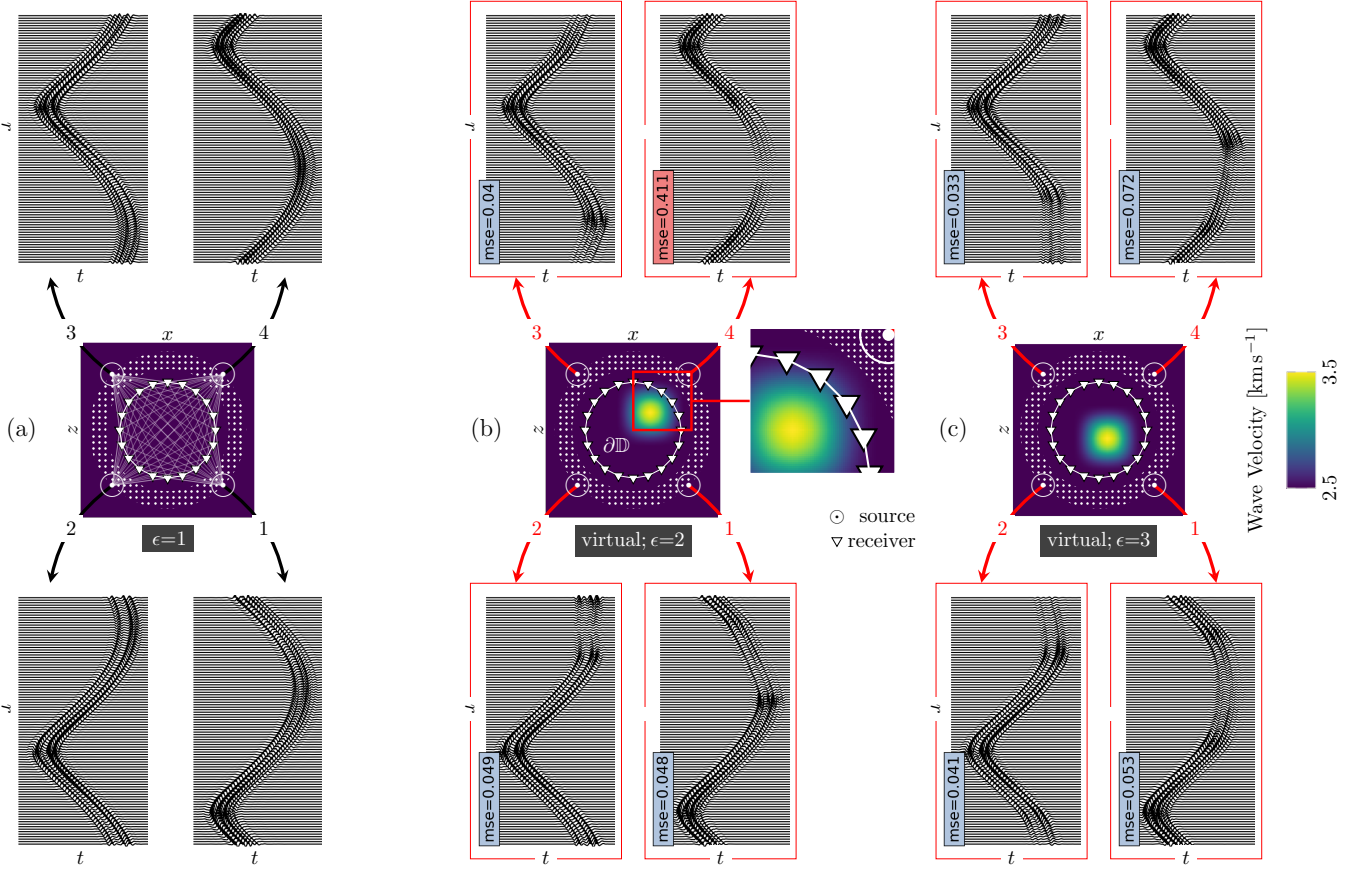


FIG. 4. Deep redatuming of waves recorded on  $\partial\mathbb{D}$  due to point sources in the dotted region. This experiment illustrates that SymAE can isolate (coherent) information on the medium (Gaussian) perturbation in its representation — however, the perturbation has to lie within  $\partial\mathbb{D}$ . a)  $X_1[1:4]$ ; original instances from the first state with a homogeneous medium. b)  $\hat{X}_{1\rightarrow 2}[1:4]$ ; virtual instances generated after swapping  $C$  with that of the second state. A high MSE in  $\hat{X}_{1\rightarrow 2}[4]$  indicates that  $C$  fails to represent the effects of the Gaussian perturbation entirely. Note that this perturbation extends beyond  $\partial\mathbb{D}$ . c)  $\hat{X}_{1\rightarrow 3}[1:4]$ ; same as (b), except a lower MSE, means that  $C$  satisfactorily represents the medium when the perturbations lie within  $\partial\mathbb{D}$ .

### Appendix C: Experiments Involving Wave Propagation

We now detail the application of SymAE in experiments involving propagation of seismic waves in the subsurface. The goal of these experiment is to monitor the time-lapse changes in the subsurface. Towards this end, seismic surveys are typically carried out once every few months to record waves from distant seismic sources that are uncontrollable (see, e.g., [27]). The duration of each survey is in the order of hours or days, during which numerous instances are recorded. As the changes in the medium are negligible during each survey, these instances can be grouped into a state with coherent information related to the medium.

For our synthetic experiments, an instance of a given state  $\epsilon$  constitutes pressure wavefield  $p(\mathbf{x}, t)$  from a finite-difference solver with absorbing boundary conditions for the acoustic wave equation:

$$\frac{1}{m^\epsilon(\mathbf{x})} \frac{\partial^2 p}{\partial t^2} - \nabla \cdot (\nabla p) = \delta(\mathbf{x} - \mathbf{x}_s) w(t). \quad (\text{C1})$$

Here,  $\mathbf{x} = [x, z]$  denotes the Cartesian coordinate vector and  $t$  denotes time. The medium is parameterized using the squared wave-velocity  $m^\epsilon(\mathbf{x})$ . Furthermore, a unique source with position  $\mathbf{x}_s$  with signature  $w(t)$  is used for modeling each instance.



## 1. Simple Illustration

Here, the subsurface varies in a  $2\text{ km} \times 2\text{ km}$  region, shown in Figs. 4a–c, across three states with  $\epsilon \in \{1, 2, 3\}$  as described in Tab. II. A unique source at  $\mathbf{x}_s = [R \cos(\theta), R \sin(\theta)]$  with signature  $w(t)$  is used for modeling each instance. The random variables  $R$  and  $\theta$  are uniformly distributed on  $[0.8, 1.0]$  km and  $[0, 2\pi]$ , respectively. The source wavelet  $w(t)$  has a duration of 0.13 s. It is sampled from a standard normal distribution and later convolved with a 25 Hz high-cut filter. After solving eq. C1, the acoustic wavefield is sampled at  $n_t = 160$  time steps and  $n_r = 100$  evenly-distributed receiver locations on a circle  $\partial\mathbb{D}$  to form an instance  $D_i^\epsilon = [p(\mathbf{x}_r, t)]_{t=1:n_t, c=1:n_r}$ . We generated 8,000 instances per state and considered a total of 6,000 datapoints (with  $n_\tau=20$ ) for training and testing. It is important to note that we chose the distribution of the forcing term in eq. C1 independently of  $\epsilon$ .

During the forward modeling, we have invariably used the same medium parameters during the forward modeling of the instances in each state. Therefore, we hypothesize that: 1. the medium parameters characterize the coherent information represented by the code  $C$ , i.e., **CEnc** encodes the information related to the entire medium in each state; 2. the forcing term characterizes the nuisance information, represented by  $N$ , of a given instance. In order to test these hypotheses numerically, we computed relative MSE between the virtual instances (generated by deep redatuming) and synthetic instances generated by appropriately choosing the medium parameters and forcing term in eq. C1. We consider redatuming of four instances,  $X_1[1:4]$  as in Fig. 4a, picked from the first state ( $\epsilon = 1$ ). We first swapped  $C$  of these instances to include the physics of wave-propagation related to the Gaussian perturbation in  $\epsilon = 2$ . The virtual instances  $\hat{X}_{1 \rightarrow 2}$  are plotted in Fig. 4b — it can be observed that source information (position and signature) was intact during redatuming, confirming that  $C$  does not represent any of the source effects. Furthermore, notice that most of the virtual instances have low MSE, for example,  $\hat{X}_{1 \rightarrow 2}[1:3]$ , indicating that  $C$  represents a significant portion of the Gaussian perturbation. However, the virtual instances with source locations close to that of  $\hat{X}_{1 \rightarrow 2}[4]$ , plotted in Fig. 4b, have high MSE. It is evident from the raypaths in Fig. 4a that only high-MSE source locations illuminate the portion of the Gaussian perturbation outside  $\partial\mathbb{D}$ . On the other hand, as the region inside  $\partial\mathbb{D}$  is coherently illuminated irrespective of the source position, we infer that SymAE’s coherent code only represents the propagation effects due to the inhomogeneities inside  $\partial\mathbb{D}$ . Towards justification of this inference, we then generated virtual instances corresponding to the state  $\epsilon = 3$ , where the Gaussian perturbation is inside  $\partial\mathbb{D}$  — as depicted in Fig. 4c, all these virtual instances have low MSE. Finally, we conclude this experiment by noting that SymAE learned to automatically recognize a portion of the medium that is coherently illuminated by the sources. Furthermore, SymAE captured salient features of the physics of wave-propagation without the need for prior information on the forward modeling.

## 2. Details on the Seismic Marmousi Experiment

We now elaborate on the experiment in Fig. 1 of the main manuscript. It involves seismic-wave propagation in a complex 2-D structural model, which is commonly known as the Marmousi model [16] in exploration seismology. These structural complexities will lead to multipath propagation. The P-wave velocity plots of this model for  $\epsilon = 1$  and  $\epsilon = 2$  are in the Figs. 5a and 5b, respectively. In this case, the forcing term represents a plane-wave source input at the bottom of the model. The source wavelet  $w(t; \tau)$  is generated by convolving a Ricker wavelet whose dominant frequency is sampled from  $\{10, 12.5, \dots, 20\}$  Hz, with a random time series (of 0.4 s duration) sampled from a standard normal distribution. As shown in the Fig. 5, the medium information is swapped from  $\epsilon = 1$  to  $\epsilon = 2$  for three instances and the other way around for remaining three instances. In all these cases, a low error indicates that the that the perturbation in the medium is well illuminated by all the planewave sources.

TABLE II.

state $\epsilon$	medium perturbation <sup>a</sup>	MSE <sup>b</sup>	virtual MSE <sup>c</sup>
1	none; homogeneous	$< 0.01$	-
2	not entirely inside $\partial\mathbb{D}$ <sup>d</sup>	$< 0.01$	high ( $> 0.3$ )
3	inside $\partial\mathbb{D}$ <sup>d</sup>	$< 0.01$	low ( $< 0.1$ )

<sup>a</sup>Gaussian perturbation <sup>b</sup> normalized mean-squared error between the true  $X$  and reconstructed  $\hat{X}$  datapoints for both training and testing <sup>c</sup>between virtual and synthetic instances after redatuming <sup>d</sup>receiver circle with center  $[0, 0]$  and radius 600 m

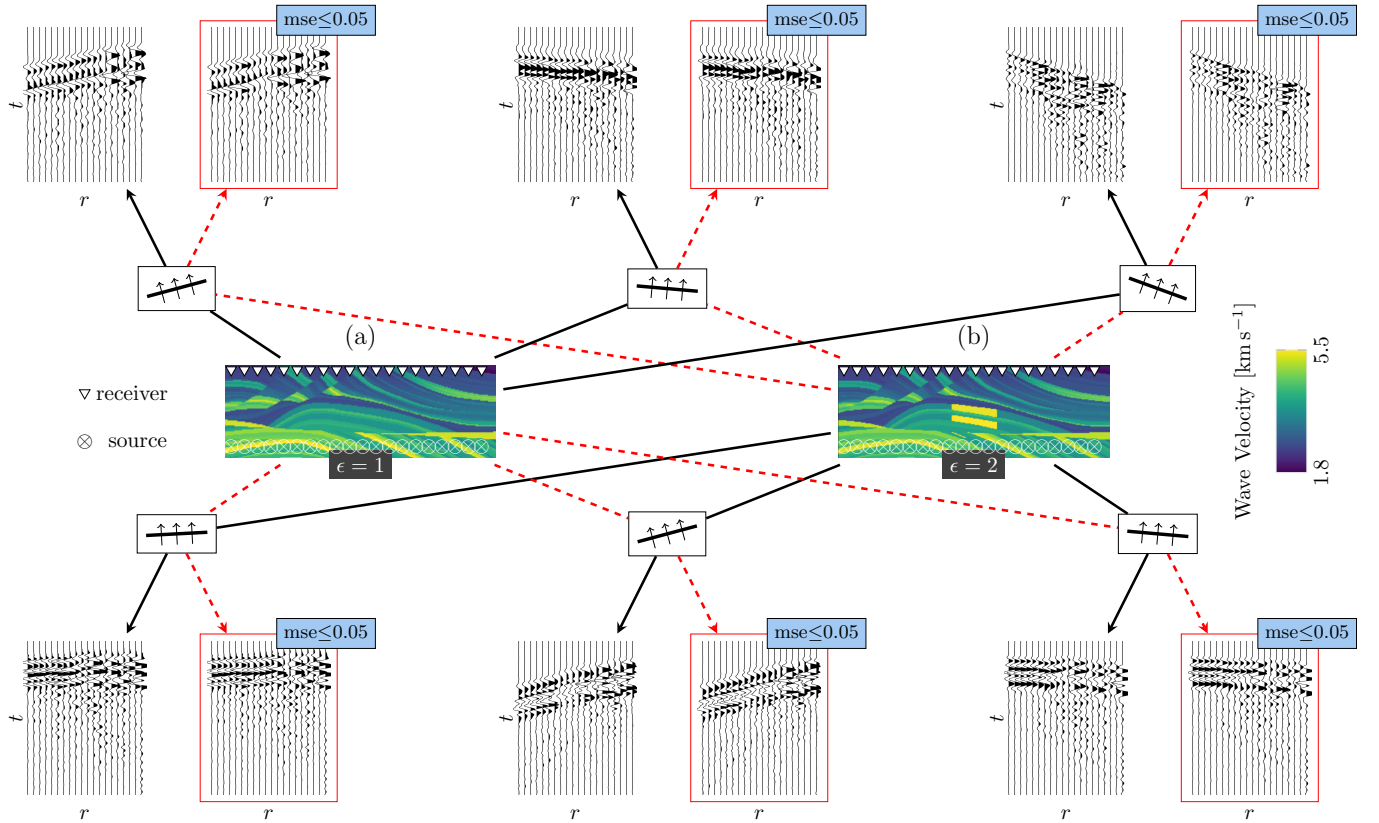


FIG. 5. Seismic Marmousi experiment where incident plane waves on the bottom of the medium undergo multipath propagation due to the complex inhomogeneities — three original instances (solid arrows) from each state are plotted reveal the complex wavefield. Note that each instance results from a planewave with a unique source wavelet and angle of arrival. Virtual instances (dashed arrows) generated after swapping  $C$  from (a) to (b) and vice versa have a low error, showcasing the success of deep redatuming.

## Appendix D: Related Work

### 1. Exploiting Physical Symmetries

SymAE heavily relies on imposing strong symmetries in the encoder to separate the latent code. The idea of using physical priors or symmetry to promote structure in the neural networks is code has been considered in various works. We mention here related work that embeds symmetries and invariances into neural network architectures: [41] embedded even/odd symmetry of a function and energy conservation into a neural network by adding special *hub* layers; [42] propose gauge equivariant CNN layers to capture rotational symmetry; [43] structures their networks following a Hamiltonian in order to learn physically conserved quantities and symmetries.

### 2. Inference With Nuisance Parameters

Ideally, the nuisance variations could be annotated within the dataset, or their effects could be eliminated or filtered from the data altogether. However, there are significant barriers towards achieving these goals. In addition, even when such a model exists, it is unclear whether there exist fundamental statistical obstructions towards consistently estimating the nuisance parameters altogether [44]. Auxiliary experimental designs may result in data to remedy this but perhaps requires instrumentation which may not be available or is prohibitively costly. We consider the setting in which the specific details of the dissimilarities across instances are rarely of interest to the domain expert. However, instead, there is the *coherent* information shared across instances. More broadly, this fits in a parameter estimation framework when a subset of the parameters are *uninteresting* or *irrelevant* to the domain expert. Although this has been considered since the inception of modern likelihood-based statistics, surprisingly, it remains an open question to

develop statistically optimal procedures; see, e.g., [45] and [46] for comprehensive literature reviews on the topic [47]. In light of this, we defer any attempts at rigorously justifying SymAE as a statistical methodology to future work. Instead, our approach is heuristic: we assume that in scientific settings, the likelihood inherits structural regularities from the underlying physics, which makes it amenable to *redatuning* the nuisance variations. Inference can then later proceed with the redatunned data. To our knowledge the theory underlying statistical redatuning has not been thoroughly investigated, perhaps since technologies for achieving realistic redatuning only appeared with the advent of modern machine learning.

### 3. VAEs: Disentanglement And Weak Supervision

Relaxing the requirement of identifiability allows the possibility of recovering instead a (possibly over-parameterized) latent code  $z = (z_1, z_2)$  which is strongly correlated with  $(\theta, \phi)$ . A contemporary approach to this problem is the variational autoencoder [48, 49]. Although it is known that the objective function is better conditioned than a deterministic autoencoding loss [50], we opt to formulate SymAE within the latter framework for simplicity. The key idea of SymAE is to partition, or structure, the latent code into attributable components  $z_1$  (for the content) and  $z_2$  (for the nuisance). This unsupervised separation into independent, explanatory coordinates (or patches of coordinates) of the latent code is referred to *unsupervised disentanglement* in the machine learning community [51]. Although “disentanglement” still lacks a rigorous mathematical definition, typical approaches towards promoting such representations have relied on statistically informed heuristics to modify the standard VAE loss function, see, e.g., the ideas proposed in  $\beta$ -VAE [52]. Surprisingly, however, [5] conducted a systematic comparison between disentanglement loss functions and noted that hyper-parameters accounted for significant variability between these techniques. Moreover, they concluded that *implicit supervision* or *inductive biases* are essential towards achieving disentanglement.

### ACKNOWLEDGMENTS

The authors thank Total SA for their support. PB is also funded via a start-up research grant from the Indian Institute of Science. PB thanks Girish from Indian Space Research Organisation and Shyama Narendranath from U R Rao Satellite Center for valuable discussions.

- 
- [1] K. Aki and P. G. Richards, *Quantitative seismology* (2002).
  - [2] J.-P. Montagner, A. Mangeney, and E. Stutzmann, *Seismology and environment* (2020).
  - [3] E. Tandberg-Hanssen and A. G. Emslie, *The physics of solar flares*, Vol. 14 (Cambridge University Press, 1988).
  - [4] S. Narendranath, P. Athiray, P. Sreekumar, B. Kellett, L. Alha, C. Howe, K. Joy, M. Grande, J. Huovelin, I. Crawford, *et al.*, Lunar x-ray fluorescence observations by the chandrayaan-1 x-ray spectrometer (c1xs): Results from the nearside southern highlands, *Icarus* **214**, 53 (2011).
  - [5] F. Locatello, S. Bauer, M. Lucic, G. Raetsch, S. Gelly, B. Schölkopf, and O. Bachem, Challenging common assumptions in the unsupervised learning of disentangled representations, in *Proceedings of the 36th International Conference on Machine Learning*, Proceedings of Machine Learning Research, Vol. 97, edited by K. Chaudhuri and R. Salakhutdinov (PMLR, 2019) pp. 4115–4124.
  - [6] G. Xu, H. Liu, L. Tong, and T. Kailath, A least-squares approach to blind channel identification, *IEEE Transactions on Signal Processing* **43**, 2982 (1995).
  - [7] J. P. Verdon, J.-M. Kendall, D. J. White, D. A. Angus, Q. J. Fisher, and T. Urbancic, Passive seismic monitoring of carbon dioxide storage at weyburn, *The Leading Edge* **29**, 200 (2010).
  - [8] R. Kamei and D. Lumley, Passive seismic imaging and velocity inversion using full wavefield methods, *SEG Technical Program Expanded Abstracts 2014*, 2273 (2014).
  - [9] K. Aki, Scaling law of earthquake source time-function, *Geophysical Journal International* **31**, 3 (1972).
  - [10] P. M. Shearer, G. A. Prieto, and E. Hauksson, Comprehensive analysis of earthquake source spectra in southern california, *Journal of Geophysical Research: Solid Earth* **111** (2006).
  - [11] P. Clark and I. Adler, Utilization of independent solar flux measurements to eliminate nongeochemical variation in x-ray fluorescence data, in *Lunar and Planetary Science Conference Proceedings*, Vol. 9 (1978) pp. 3029–3036.
  - [12] C. Aerts, J. Christensen-Dalsgaard, and D. W. Kurtz, *Asteroseismology* (Springer Science & Business Media, 2010).
  - [13] G. Handler, *Asteroseismology*, arXiv preprint arXiv:1205.6407 (2012).
  - [14] N. Samus, O. Durlevich, *et al.*, VizieR online data catalog: Combined general catalogue of variable stars (samus+ 2004), *VizieR Online Data Catalog*, II (2004).

- [15] W. W. Campbell and W. Wright, A list of nine stars whose velocities in the line of sight are variable., *The Astrophysical Journal* **12** (1900).
- [16] A. Brougois, M. Bourget, P. Lailly, M. Poulet, P. Ricarte, and R. Versteeg, Marmousi, model and data, in *EAEG workshop-practical aspects of seismic data inversion* (European Association of Geoscientists & Engineers, 1990) pp. cp–108.
- [17] Y. Mirsky, T. Mahler, I. Shelef, and Y. Elovici, Ct-gan: Malicious tampering of 3d medical imagery using deep learning, in *28th USENIX Security Symposium (USENIX Security 19)* (USENIX Association, Santa Clara, CA, 2019) pp. 461–478.
- [18] S. Suwajanakorn, S. M. Seitz, and I. Kemelmacher-Shlizerman, Synthesizing obama: Learning lip sync from audio, *ACM Trans. Graph.* **36**, 10.1145/3072959.3073640 (2017).
- [19] C. Bregler, M. Covell, and M. Slaney, Video rewrite: Driving visual speech with audio, in *Proceedings of the 24th Annual Conference on Computer Graphics and Interactive Techniques, SIGGRAPH '97* (ACM Press/Addison-Wesley Publishing Co., USA, 1997) p. 353–360.
- [20] F. Locatello, B. Poole, G. Raetsch, B. Schölkopf, O. Bachem, and M. Tschannen, Weakly-supervised disentanglement without compromises, in *Proceedings of the 37th International Conference on Machine Learning*, Proceedings of Machine Learning Research, Vol. 119, edited by H. D. III and A. Singh (PMLR, 2020) pp. 6348–6359.
- [21] In previous work, we used focusing constraints [53] to maximize this dissimilarity and regularize blind deconvolution.
- [22] K. Wapenaar, Retrieving the elastodynamic Green’s function of an arbitrary inhomogeneous medium by cross correlation, *Physical Review Letters* **93**, 254301 (2004).
- [23] G. T. Schuster and M. Zhou, A theoretical overview of model-based and correlation-based redatuming methods, *Geophysics* **71**, SI103 (2006).
- [24] G. Schuster, *Seismic Interferometry*, Vol. 9780521871 (Cambridge University Press Cambridge, 2009) pp. 1–260.
- [25] W. A. Mulder, Rigorous redatuming, *Geophysical Journal International* **161**, 401 (2005).
- [26] K. Wapenaar, J. Thorbecke, J. Van Der Neut, F. Broggini, E. Slob, and R. Snieder, Marchenko imaging, *Geophysics* **79**, WA39 (2014).
- [27] A. Mordret, N. M. Shapiro, and S. Singh, Seismic noise-based time-lapse monitoring of the Valhall overburden, *Geophysical Research Letters* **41**, 4945 (2014).
- [28] S. A. De Ridder, B. L. Biondi, and R. G. Clapp, Time-lapse seismic noise correlation tomography at Valhall, *Geophysical Research Letters* **41**, 6116 (2014).
- [29] J. van der Neut and K. Wapenaar, Adaptive overburden elimination with the multidimensional Marchenko equation, *Geophysics* **81**, T265 (2016).
- [30] C. Doersch, Tutorial on variational autoencoders, arXiv preprint arXiv:1606.05908 (2016).
- [31] We choose to use a deterministic autoencoding strategy for simplicity. It is possible to formalize the ideas in this paper using the variational autoencoding framework.
- [32] J. Klys, J. Snell, and R. Zemel, Learning latent subspaces in variational autoencoders, arXiv preprint arXiv:1812.06190 (2018).
- [33] B. Dai and D. Wipf, Diagnosing and enhancing VAE models, 7th International Conference on Learning Representations, ICLR 2019 , 1 (2019), arXiv:1903.05789.
- [34] M. Abadi, A. Agarwal, P. Barham, E. Brevdo, Z. Chen, C. Citro, G. S. Corrado, A. Davis, J. Dean, M. Devin, S. Ghemawat, I. Goodfellow, A. Harp, G. Irving, M. Isard, Y. Jia, R. Jozefowicz, L. Kaiser, M. Kudlur, J. Levenberg, D. Mane, R. Monga, S. Moore, D. Murray, C. Olah, M. Schuster, J. Shlens, B. Steiner, I. Sutskever, K. Talwar, P. Tucker, V. Vanhoucke, V. Vasudevan, F. Viegas, O. Vinyals, P. Warden, M. Wattenberg, M. Wicke, Y. Yu, and X. Zheng, *TensorFlow: Large-Scale Machine Learning on Heterogeneous Distributed Systems*, Tech. Rep. (2016) arXiv:1603.04467.
- [35] We provided more architectural details in the appendix.
- [36] M. Zaheer, S. Kottur, S. Ravanbakhsh, B. Póczos, R. Salakhutdinov, and A. J. Smola, Deep sets, *Advances in Neural Information Processing Systems* , 3392 (2017), arXiv:1703.06114.
- [37] M. Ilse, J. M. Tomczak, and M. Welling, Attention-based deep multiple instance learning, 35th International Conference on Machine Learning, ICML 2018 **5**, 3376 (2018), arXiv:1802.04712.
- [38] N. Srivastava, G. Hinton, A. Krizhevsky, I. Sutskever, and R. Salakhutdinov, Dropout: a simple way to prevent neural networks from overfitting, *The journal of machine learning research* **15**, 1929 (2014).
- [39] S. Wang and C. Manning, Fast dropout training, in *international conference on machine learning* (PMLR, 2013) pp. 118–126.
- [40] D. P. Kingma, T. Salimans, and M. Welling, Variational dropout and the local reparameterization trick, *Advances in neural information processing systems* **28**, 2575 (2015).
- [41] M. Mattheakis, P. Protopapas, D. Sondak, M. Di Giovanni, and E. Kaxiras, Physical Symmetries Embedded in Neural Networks, arXiv:1904.08991 [physics] (2019), arXiv:1904.08991.
- [42] T. S. Cohen, M. Weiler, B. Kicanaoglu, and M. Welling, Gauge equivariant convolutional networks and the icosahedral CNN, 36th International Conference on Machine Learning, ICML 2019 **2019-June**, 2357 (2019), arXiv:1902.04615.
- [43] S. Greydanus, M. Dzamba, and J. Yosinski, Hamiltonian Neural Networks, arXiv (2019), 1906.01563.
- [44] J. Neyman and E. L. Scott, Consistent estimates based on partially consistent observations, *Econometrica* **16**, 1 (1948).
- [45] D. Basu, On the elimination of nuisance parameters, *Journal of the American Statistical Association* **72**, 355–366 (1977), publisher: Taylor & Francis.
- [46] T. Lancaster, The incidental parameter problem since 1948, *Journal of Econometrics* , 23 (2000).
- [47] For example, it is known that maximum likelihood estimation may not necessarily be consistent [46].
- [48] D. P. Kingma and M. Welling, Auto-encoding variational bayes, 2nd International Conference on Learning Representations, ICLR 2014 - Conference Track Proceedings , 1 (2014), arXiv:1312.6114.

- [49] D. J. Rezende, S. Mohamed, and D. Wierstra, Stochastic backpropagation and approximate inference in deep generative models, in *Proceedings of the 31st International Conference on Machine Learning*, Proceedings of Machine Learning Research, Vol. 32, edited by E. P. Xing and T. Jebara (PMLR, Beijing, China, 2014) pp. 1278–1286.
- [50] B. Dai, Y. Wang, J. Aston, G. Hua, and D. Wipf, Connections with robust pca and the role of emergent sparsity in variational autoencoder models, *Journal of Machine Learning Research* **19**, 1 (2018).
- [51] A. Achille and S. Soatto, Emergence of invariance and disentanglement in deep representations, arXiv:1706.01350 [cs, stat] (2018), arXiv: 1706.01350.
- [52] I. Higgins, L. Matthey, A. Pal, C. Burgess, X. Glorot, M. Botvinick, S. Mohamed, and A. Lerchner, beta-vae: Learning basic visual concepts with a constrained variational framework, in *ICLR* (2017).
- [53] P. Bharadwaj, L. Demanet, and A. Fournier, Focused blind deconvolution, *IEEE Transactions on Signal Processing* **67**, 3168 (2019).